Experimental and Numerical Investigations of Fundamental Radiation Mechanisms in PCB Designs with Attached Cables

D. M. Hockanson, *C.-W. Lam, J. L. Drewniak, T. H. Hubing, & T. P. Van Doren
Electromagnetic Compatibility Laboratory
Department of Electrical Engineering
University of Missouri-Rolla
Rolla, MO 65401
and
*Quad Design Technology
Camarillo, CA 93010

Abstract

Stacked-card and modules-on-backplane printed circuit board geometries are advantageous for conserving real-estate in many designs. Unfortunately, at high frequencies, current-driven noise sources may develop at the connector. The connector may effectively drive the daughter-card against the mother-board and attached cables, resulting in common-mode radiation. The connector geometry can be modified to reduce the level of the effective noise-source when high frequencies are routed between the mother-board and daughter-card. Current speeds and PCB board sizes result in geometries that are of significant dimensions in terms of wavelength at the upper frequency end of the signal spectrum. Geometries are then of sufficient electrical extent to be effective EMI antennas. The resonant lengths of the EMI antennas may, however, be quite removed from the typical dipole resonances of half-wavelength intervals. The Finite-Difference Time-Domain method can be used to numerically analyze the printed circuit-board geometries, determine antenna resonances, and investigate EMI noise source mechanisms.

1 Introduction

The evolution of the electronics industry has placed size minimization among the attributes determining acceptable product designs. Stacked-card and modules-on-backplane printed-circuit board (PCB) configurations have proven to be successful methods for conserving real-estate. Unfortunately, connectors provide an opportunity for noise to be coupled to other systems through magnetic- and electric-field coupling, and to the environment through electromagnetic radiation. Mechanisms by which signals get from IC sources to locations associated with noise-sources have been demonstrated experimentally [1], [2]. The noise-sources can be reduced to two classes: voltage-driven sources, and current-driven sources [1]. The current-driven noise-source is of particular interest when dealing with connector geometries of PCBs and is reviewed herein for this application.

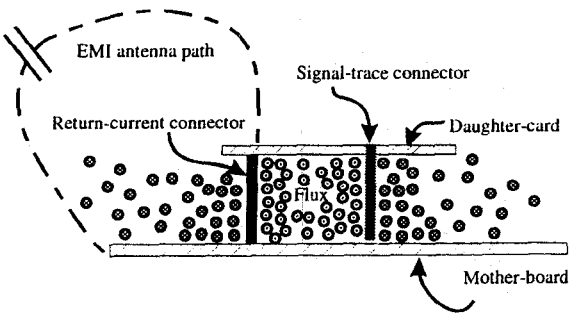

Figure 1: Cross section of a stacked-card PCB configuration showing the flux coupling the EMI antenna path.

Figure 1 shows a two - dimensional view of a stacked-card configuration with a daughter-card and mother-board. The trace is routed along the mother-board and onto the daughter-card where it is terminated. The return-current path between the daughter-card reference plane and the mother-board reference plane is a conducting stub located 5 cm from the trace. Another return path may be considered the "EMI antenna" path depicted in the figure as a capacitor (displacement current). The connection between the daughter-card and mother-board is comprised of a large loop where the flux shown in Figure 1 is circling the trace conductor and the return-

0-7803-3207-5/96/$5.00 © 1996 IEEE

current conductor. Because the return-current conductor is so removed from the location of the trace, a significant amount of the flux wraps around the return-current connector which results in a potential difference. This coupling is the noise source and is referred to as a current-driven voltage source. Typically the impedance represented by the EMI antenna loop is very large, and little current is driven along the antenna return path. However, when the geometry is of resonant dimension, the impedance of the loop containing the EMI antenna may be significantly less than 100Ω, and the induced common-mode currents can result in radiation. The flux which wraps around the return-current connector can be modeled as a partial-inductance. By constructing a connector which minimizes this partial-inductance, the effect of a current-driven source at the connector can be reduced. In the following section, a stacked-card PCB model is experimentally evaluated with three different connector configurations between the daughter-card and mother-board.

The EMI antennas on the PCB are not easily evaluated. The antenna does not usually consist of simply wires and cables. Consequently, finding the frequency for which the "length" of the antenna is a half-wavelength is not an accurate solution for the first resonance frequency. Intuitively, the presence of a large plate as one of the conductors provides more capacitance to the antenna, thereby shifting the resonances down in frequency. FDTD can model these structures and predict the resonance frequencies for complicated PCB geometries.

2 Stacked-card Configuration

The connector geometry linking a daughter-card and mother-board must be carefully designed for the bandwidth associated with the signals being communicated through the connector. The modules-on-backplane configuration has been numerically studied using FDTD with reasonable agreement with experimental results [3]. The EMI associated with a stacked-card PCB design was studied here by measuring the common-mode current induced on the connecting cable. Figure 2 shows the geometry studied. A trace was routed from the mother-board to the daughter-card and terminated. Three different schemes for connecting the mother-board reference plane to the daughter-card reference plane were investigated. Connector 1 was constructed by connecting the daughter-card and mother-board reference planes with a wire located 5 cm from the trace conductor. Connector 2 located the wire 2 mm from

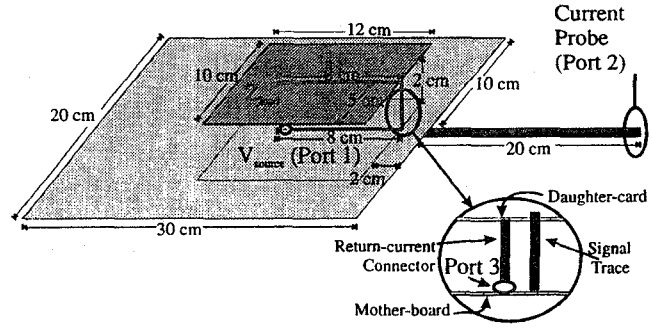

Figure 2: Geometry of the stacked-card geometry studied in this investigation. Connector region is exploded to show location of Port 3.

the trace conductor. In Connector 3, a conducting strip 2.5 cm wide was centered behind the trace conductor. The ends of the strip were well connected to the reference planes resulting in a microstrip-type geometry.

S_{21} was measured with the locations of Port 1 (voltage source for signal trace) and Port 2 (current-probe on cable) as shown in Figure 2. The response of the current-probe was included in the calibration of the network analyzer. Therefore, S_{21} is defined here as $\frac{50 I_{common-mode}}{V_{source}}$. Input impedance was computed at Port 1 and at a port (Port 3) between the return-current connector (2 mm from trace) and the mother-board. The end of the attached cable was terminated on a square aluminum plate (60 cm X 60 cm) to isolate the device from the cable dressing of the network analyzer. The low-frequency response of the model with a short-circuited trace should behave as an inductor when observed from Port 1. The measured inductances of the signal circuit with the reference connector located 5 cm from the trace, 2 mm from the trace, and the microstrip connector were 80 nH, 56 nH, and 50 nH, respectively. The capacitance of the signal circuit could be calculated by observing the low-frequency input-impedance results for an open-circuited trace. The capacitance between trace and reference for all three connector geometries was 15 pF.

Figure 3 shows the magnitude of S_{21} from 40 MHz to 600 MHz for the stacked-card geometry with a short-circuit trace. Two distinct peaks were observed indicating higher radiation from common-mode currents. The first common-mode resonance was at approximately 90 MHz and the second was around 300 MHz.

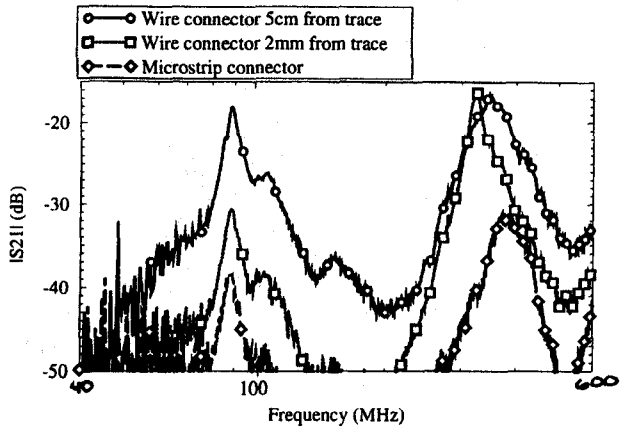

Figure 3: $|S_{21}|$ results for the stacked-card configuration with a short-circuited trace (on daughter-card) for three different connector geometries.

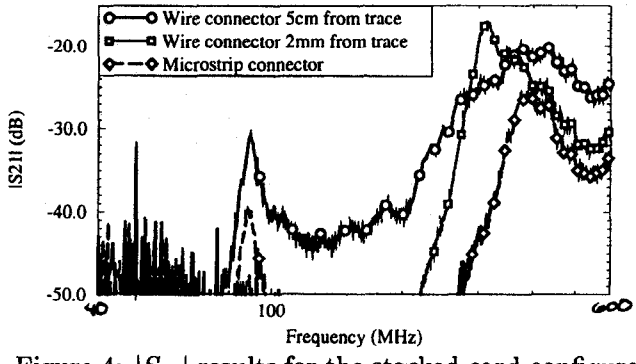

Figure 4: $|S_{21}|$ results for the stacked-card configuration with an open-circuited trace (on daughter-card) for three different connector geometries.

2.1 First Resonance Observations

Figure 4 shows the common-mode current on the cable when the trace was open-circuited. At lower frequencies, the input impedance (of the signal circuit) measured at Port 1 was lower for the short-circuit case than for the open-circuit case ($j\omega L_{circuit} < 50\Omega$, $\frac{1}{j\omega C_{circuit}} > 100\Omega$, for $f < 100MHz$). Consequently, the signal current was higher for the short-circuit case resulting in a larger noise-source. Comparing Figures 3 and 4, the common-mode current with an open-circuit trace was ≈12 dB less than with a short-circuit trace. This decrease in common-mode current supports a current-driven mechanism for the first resonance.

As the connector geometry is changed from Cases 1 to 3, the noise-source magnitude is changed because of lower partial inductance. The partial-inductance represented by the flux wrapping around the return-current connector in Figure 1 is decreasing as the connector geometry is changed from a wire 5 cm from the trace, to a wire 2 mm from the trace, to a microstrip geometry. Hence, the level of common-mode current decreases as the partial-inductance decreases as seen in Figure 3. The self-inductance of the connector plays only a small role in the noise-source. The larger impedance exhibited by a larger self-inductance may lessen the drive current which results in a current-driven source. But changing the connector geometry to limit the partial-inductance reduces the noise-source magnitude more significantly. This is evident in Figure 3 where the self-inductance differs by only several nH between the microstrip connector and the return-current connector at 2 mm. The common-mode current was reduced by approximately 8 dB because the microstrip connector reduces the partial-inductance. Unexplainably, the $|S_{21}|$ results for the open- and short-circuit trace were virtually unchanged at the first primary resonance, for the microstrip connector configuration. This result may be linked to the noise-source which drives the mother-board–cable EMI antenna.

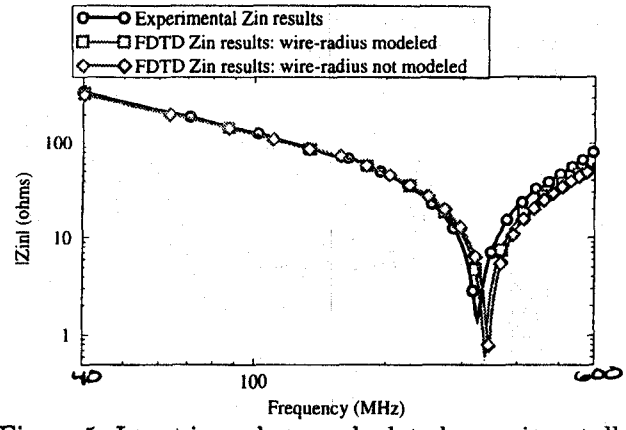

Figure 5: Input impedance calculated experimentally and numerically with FDTD as observed at Port 3.

Initially, the EMI antenna for the first resonance might be expected as the daughter-card being driven against the cable. However, this does not appear to be the case. The self-inductance represented by the return-current connector should change as the connector is changed from a wire to a microstrip geometry. The self-inductance change should shift the resonance frequency, which is not apparent in Figure 3. However, it could be argued that the connector contribution to the antenna is negligible. Figure 5 shows the input impedance at Port 3, both measured and computed using FDTD. Below 100 MHz the input impedance looks capacitive and is near 100 Ω and above. No antenna resonance occurs in the proxim-

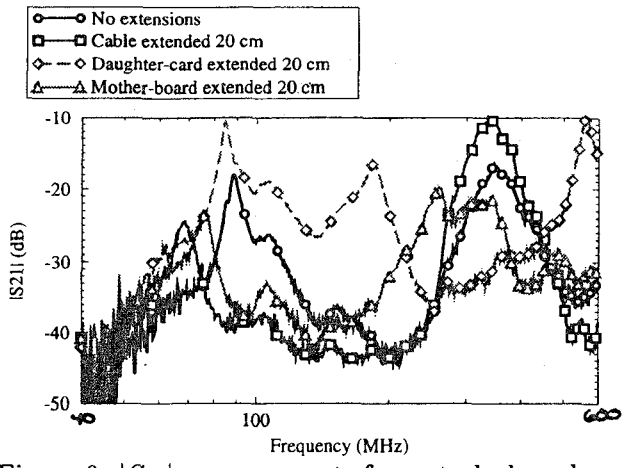

Figure 6: $|S_{21}|$ measurements for a stacked-card configuration with the return-current connector located 5 cm from the trace. The trace was short-circuited on the daughter-card. The EMI antennas were modified to determine the common-mode radiation contributors.

ity of 90 MHz although considerable common-mode current is being driven onto the cable as shown in Figure 3. Figure 6 shows changes in $|S_{21}|$ which resulted from changing the lengths of the EMI antennas. All the results shown in Figure 6 were measured with the return-current connector located 5 cm from a short-circuited trace. Extending the cable 20 cm shifted the lower resonance frequency down 20 MHz. This shift indicated that the attached cable was a part of the EMI antenna. Extending the daughter-card 20 cm changed the resonance frequency a few MHz, but not as much as would be expected if the daughter-card were a significant part of the EMI antenna. Extending the mother-board 20 cm shifted the resonance frequency down 10 MHz, which indicates that the mother-board is another part of the EMI antenna. The resonance frequency with the extended mother-board is not expected to be the same as the resonance frequency with the extended cable because the electrical extent was changed more significantly when the cable was extended than when the mother-board was extended due to the large width of the mother-board. Figure 6 also depicts a 5 dB change in the level of common-mode current at the lower resonance frequency when the primary EMI antenna (mother-board–cable) is altered. The change in the level of common-mode current between the control case and the 20 cm mother-board extension or 20 cm cable extension may be due to a change in input impedance at resonance when the electrical extent of the EMI antenna is changed. The daughter-card extension resulted in an 8 dB increase in common-

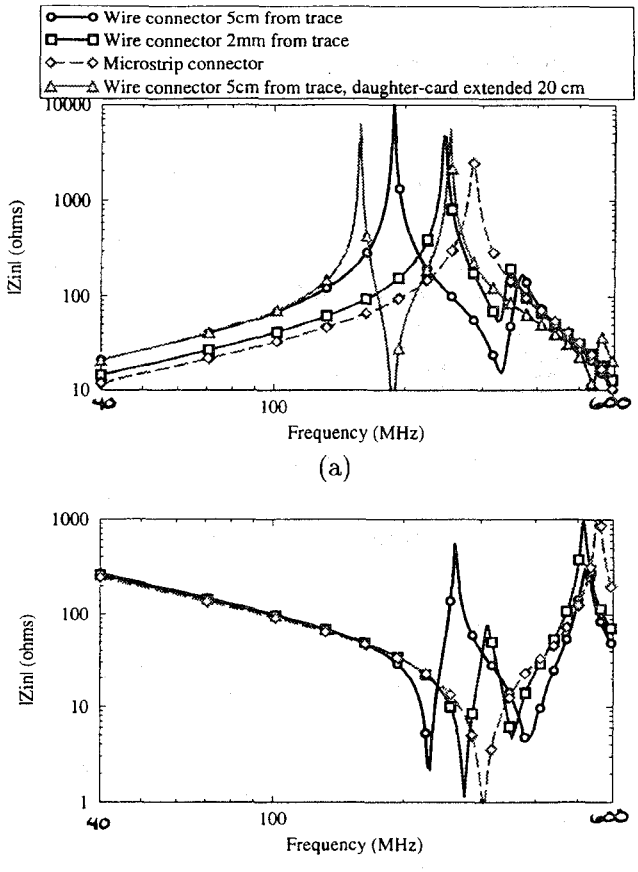

Figure 7: Input impedance at Port 1 for three connector geometries with a) short-circuited trace and b) open-circuited trace.

mode current at the first resonance. Figure 7 shows precision input impedance measurements (HP 4291A Impedance/Material Analyzer) at Port 1 for the short- and open-circuited traces (on daughter-card) for the three different connector geometries as well as the extended daughter-card (short-circuit trace only). Figure 7a shows that at 90 MHz the input impedance from Port 1 is the same with or without the extended daughter-card. The differential-mode current should then be the same for both cases, and the noise-source the same magnitude. Figure 8 shows the input impedance at Port 3 when the daughter-card and mother-board are extended. However Figure 8 shows that the input impedance at Port 3 was different for the two daughter-card configurations. The ratio of common-mode currents for the two cases is

$$\frac{I_{cm}^{extension}}{I_{cm}^{noextension}} = \frac{\frac{V_{noise}}{Z_{in}^{extension}}}{\frac{V_{noise}}{Z_{in}^{noextension}}}.$$

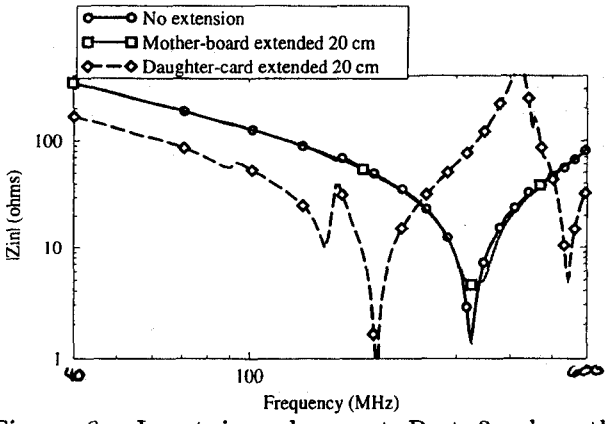

Figure 8: Input impedance at Port 3 when the daughter-card and mother-board were extended compared to the stacked-card configuration without extensions.

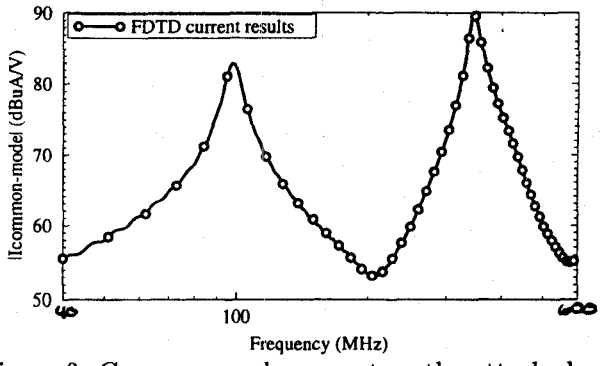

Figure 9: Common-mode current on the attached cable normalized to a voltage-source at Port 3 as computed by FDTD.

From Figure 8, $|Z_{in}^{extension}|$ was approximately 60 Ω, and $|Z_{in}^{noextension}|$ was approximately 150 Ω. The ratio of common-mode currents in dB can then be expressed as

$$\begin{aligned} I_{cm}^{extension}(dB) - I_{cm}^{noextension}(dB) &= 20\log\left(\frac{I_{cm}^{extension}}{I_{cm}^{noextension}}\right) \\ &= 20\log\left(\frac{Z_{in}^{noextension}}{Z_{in}^{extension}}\right) \\ &= 20\log 2.5 = 7.95dB, \end{aligned}$$

which is the increase in $|S_{21}|$ in Figure 6. The method by which the energy couples from the return-current connector to the mother-board–cable is currently not well understood. Characterization of the coupling mechanism is being pursued through further experimental and numerical studies.

2.2 Second Resonance Observations

The second primary resonance that occurs around 300 MHz is a result of the daughter-card being driven against the mother-board. Experimentally and numerically a resonance occurs (Figure 5 and Figure 3) that corresponds to the daughter-card being driven against the mother-board. The experimental results were measured by placing Port 3 between the bottom of the return-current connector and the mother-board. The FDTD results were generated in a similar fashion. First, the input-impedance was computed by modeling the return-current stub as a perfect electric conductor by setting the axial electric-field component to zero. The FDTD predicted resonance frequency differed from the experimental results by approximately six percent. The low-frequency input-impedance results follow the experimental results very closely, suggesting that the mother-board and daughter-card which were modeled as perfectly conducting sheets were well modeled. After the resonance the slope does not follow the experimental results as well, indicating that the inductance associated with the resonance was not adequately modeled. A subcellular thin-wire algorithm was used to model the wire radius with a higher degree of accuracy [4], [5]. The resonance frequency computed by FDTD was then determined with less than four percent error when compared to the experimental results. Figure 9 shows the common-mode current on the attached cable normalized to a voltage-source place at Port 3 as computed by FDTD. The computed resonance frequencies agree well with those of Figures 3 and 4 although the return-current connector was not modeled with the thin-wire algorithm. The thin-wire algorithm uses quasi-static approximations which are reasonable for long wires, but may be less applicable here. The return-current connector was 2 cells long which may have been too short for accurate modeling with the thin-wire algorithm. Finer discretization may yield better results.

The measured $|S_{21}|$ in Figure 6 shows that the extension of the attached cable resulted in no change in the second resonance frequency. This indicates that the cable plays a minimal role in the second resonance. When the mother-board is extended the resonance frequency changes about 25 MHz, however when the daughter-card is extended the resonance frequency changes about 100 MHz. The first resonance of a dipole antenna may be modeled as a series LC resonance. Therefore as the capacitance is increased, the resonance frequency is shifted lower in frequency. The capacitance change due to the mother - board extension is small compared to the change in the capacitance when the daughter-card is extended.

Figure 8 shows the input impedance at Port 3

when the daughter-card and mother-board are extended. When the mother-board is extended, the resonance shifts down approximately 10 MHz as a result of increasing the capacitance of the EMI antenna slightly. However, when the daughter-card is extended the resonance frequency shifts down over 100 MHz. The large shift results from substantially increasing the parallel-plate capacitance of the EMI antenna. At 550 MHz another resonance results (see Figures 6 and 8) that similarly drives current on the attached cable.

The noise-source is current-driven at the second resonance as well. At resonance the input impedance is only a few ohms. The flux which coupled to the external environment generates an emf which drives relatively high levels of common-mode current from the daughter-card to the mother-board because of the low EMI antenna input impedance. The coupling between the mother-board–cable EMI antenna and the daughter-card–mother-board EMI antenna is presently not well understood.

Figure 7 shows the input impedance measured at Port 1 for the short- and open-circuited traces for the three different connector geometries as well as the extended daughter-card (short-circuit trace only). As the connector-geometry was shifted from the case with the most self-inductance (return-current connector 5 cm from the trace) to the least self-inductance (microstrip connector), the pole-zero combination in Figure 7a was shifted up in frequency. A similar response was noted for the open-circuit case as shown in Figure 7b. Of particular interest are the cases where the microstrip connector was implemented. The zero-pole resonance at approximately 350 MHz is completely missing for the short-circuit trace. Similarly the pole-zero resonance following the initial zero has been removed in the open-circuit case. This may be a result of better impedance matching of the trace at higher-frequencies. The microstrip connector appears electrically similar to the trace over the reference-plane. The result is a trace which appears continuous, as opposed to a trace with a lumped-element load at the connector, followed by another trace. The effect on common-mode current, however, seems minimal. The EMI antenna resonance should shift up in frequency when the microstrip connector is implemented because of the lower partial-inductance imparted to the EMI antenna by the connector. This is evident in both Figures 3 and 4 where the second resonance has been shifted approximately 80 MHz from the resonance shown in Figure 5, where the return-current connector was a wire.

3 Summary & Conclusion

A stacked-card PCB configuration was investigated experimentally and numerically with FDTD. Two primary resonances were observed between 40 MHz and 600 MHz which contributed to common-mode radiation. Current-driven sources excite the EMI antennas. Modifications in the connector-geometry which connects the mother-board to the daughter-card suppress the EMI radiation by more than 20 dB by reducing the magnitude of the noise-sources. However, the primary noise-source was found to couple to a secondary-noise source. Initial studies indicate that the EMI antennas in the stacked-card configuration are coupled in a manner that may increase the complexity of the problem significantly. Further experimental and computational modeling (FDTD and equivalent circuit) is necessary to determine the extent and effects of the antenna and noise-source coupling mechanisms.

References

[1] J. L. Drewniak, T. H. Hubing, and T. P. Van Doren, "Investigation of fundamental mechanisms of common-mode radiation from printed circuit boards with attached cables", in *1994 IEEE International Symposium on Electromagnetic Compatibility*. IEEE Electromagnetic Compatibility Society, August 1994, pp. 110–115.

[2] J. R. Bergervoet, "EMC measurements and models connecting the system level with the module level", *Phillips Journal of Research*, vol. 48, pp. 63–80, 1994.

[3] K. Li, M. A. Tassoudji, S. Y. Poh, M. Tsuk, R. T. Shin, and J. A. Kong, "FD-TD analysis of electromagnetic radiation from modules-on-backplane configurations", *IEEE Transactions on Electromagnetic Compatibility*, vol. 37, pp. 326–332, August 1995.

[4] D. M. Hockanson, J. L. Drewniak, T. H. Hubing, and T. P. Van Doren, "FDTD modeling of common-mode radiation from cables", *IEEE Transactions on Electromagnetic Compatibility*, accepted for publication January 1996.

[5] A. Taflove, K. Umashankar, B. Beker, F. Harfoush, and K. Yee, "Detailed FD-TD analysis of electromagnetic fields penetrating narrow slots and lapped joints in thick conducting screens", *IEEE Transactions on Antennas and Propagation*, vol. 36, pp. 247–257, February 1988.